Journal of Marine Science and Application (2026) 25: 110-121
https://doi.org/10.1007/s11804-025-00696-3

RESEARCH ARTICLE

Wave Energy System Combined by a Heaving Box and a Perforated Flexible Membrane Wall

Sarat Chandra Mohapatra[1] **and C. Guedes Soares**[1]

Received: 06 November 2024 / Accepted: 20 March 2025

Abstract

An analytical model of a floating heaving box integrated with a vertical flexible porous membrane placed right next to the box applications to wave energy extraction and breakwater systems is developed under the reduced wave equation. The theoretical solutions for the heave radiating potential to the assigned physical model in the corresponding zones are attained by using the separation of variables approach along with the Fourier expansion. Applying the matching eigenfunction expansion technique and orthogonal conditions, the unknown coefficients that are involved in the radiated potentials are determined. The attained radiation potential allows the computation of hydrodynamic coefficients of the heaving buoy, Power Take-Off damping, and wave quantities. The accuracy of the analytical solution for the hydrodynamic coefficients is demonstrated for different oblique angles with varying numbers of terms in the series solution. The current analytical analysis findings are confirmed by existing published numerical boundary element method simulations. Several numerical results of the hydrodynamic coefficients, power capture, power take-off optimal damping, and transmission coefficients for numerous structural and physical aspects are conducted. It has been noted that the ideal power take-off damping increases as the angle of incidence rises, and the analysis suggests that the ability to capture waves is more effective in shallower waters compared to deeper ones.

Keywords Analytical model; Heaving buoy; Flexible membrane perforated wall; Boundary element method code; Power take-off; Power capture

1 Introduction

In recent decades, research on wave energy extraction has aimed to maximize energy capture while keeping costs manageable. Nonetheless, only a limited number of wave energy converters (WECs) are currently applicable in practical engineering due to their cost-effectiveness (Wang and Dong, 2023; Han and Dong, 2021). A recommendation is to combine WECs with various marine structures (Hallak and Guedes Soares, 2025), such as offshore platforms and breakwaters, while considering environmental factors like angled waves and currents, to develop a multi-functional system that can lower construction and design expenses.

The placement of this present integrated wave energy system (WES) in coastal zones is extremely beneficial for several grounds, which contribute to its appeal. These reasons include: i) the availability of existing structures like breakwaters and seawalls that can be leveraged for the integrated WES to extract wave energy due to the heaving buoy, ii) the reflected waves from these structures that enhance wave energy extraction due to the porous-effect parameter that dissipates wave energy, and iii) significantly reduced construction and design costs in comparison to deep sea locations. Therefore, to save the fabricating cost of the WECs (Wang et al., 2022b; Zhao et al., 2019; Vicinanza et al., 2019; Mustapa et al., 2017), the present integrated WES can be used in practical engineering.

Emerging studies are exploring a new WES design that integrates buoys or oscillating water columns (OWCs) via

Article Highlights

- In order for wave energy and a breakwater system to be a viable energy option and coastal protection, a wave energy system combined with a floating box and a perforated wall developed.
- The analytical solution is obtained, and the computation of hydrodynamic coefficients of the heaving buoy, Power Take-Off damping, and wave quantities.
- The accuracy of the obtained solution is demonstrated and the present findings are validated by numerical boundary element method simulations.
- The model efficiency is analyzed through the hydrodynamic coefficients, power capture, power take-off optimal damping, and wave quantities.

✉ Sarat Chandra Mohapatra
sarat.mohapatra@centec.tecnico.ulisboa.pt

[1] Center for Marine Technology and Ocean Engineering (CENTEC), Instituto Superior Técnico, Universidade de Lisboa, Lisboa 1049-001, Portugal

either floating or breakwaters that are fixed (Rezanejad and Guedes Soares, 2018). Numerical and theoretical approaches have been employed to analyze these models. The theoretical studies on the hydrodynamic efficiency of hybrid wave energy extraction (WEE) systems (Wang and Dong, 2021, 2023). These systems consisted of a toroidal oscillating body, a coordinated porous cylindrical structure, and a toroidal oscillating buoy. All these components were positioned on a bottom heaving WEC located centrally within a semi-circular aperture in a vertical solid breakwater. Proximity to a rigid rear wall significantly amplifies horizontal forces on a WEC and the wall itself. Significantly, these effects occur at frequencies that match the piston mode gap and the heave resonance frequencies. Using an analytical approach and subjected to oblique waves, the influence of incident wave angle on a floating structure with no motion of rectangular geometry close to a vertical wall with a stepped bottom was investigated in Bhattacharjee and Guedes Soares (2011). Schay et al. (2013) used the commercial software WAMIT to simulate various floater shapes for heaving point absorbers positioned close to a vertical rigid wall, subsequently analyzing the resulting forces and hydrodynamic coefficients. Using a matching technique, Wang et al. (2022a) analyzed a WEE system comprising a heaving buoy and a porous wall, designed to work cohesively.

Hsu and Wu (1997) investigated the effect of a rigid vertical wall and bottom sill on the wave quantities and hydrodynamic characteristics pertaining to a rectangular floating structure (Shen et al., 2005). It was found a positive correlation between sill height and reflection coefficient in different water depths; conversely, the transmission coefficient decreased as sill height increased. The effectiveness of a floating breakwater (FB), involving mooring cables and a vertical wall was investigated through the wave quantity by Elchahal et al. (2008). To broaden the effective frequency bandwidth, Ning et al. (2017) developed an FB featuring a dual-pontoon design and then investigated the impact of WEC power take-off (PTO) damping on wave characteristics, response amplitude operator (RAO), and performance of the resulting integrated WEC configuration. Rezanejad and Guedes Soares (2021) examined the hydrodynamic efficiency of an innovative floating OWC device consisting of two chambers placed in the front and back regions in the upstream region.

Zhang et al. (2020) examined how wave reflection affects the hydrodynamic behavior of a combined FB and WEC and their results demonstrated that the inclusion of the wall significantly changed the system's hydrodynamic properties, energy conversion efficiency, and wave reduction performance. Ji et al. (2021) introduced a novel design for a reversed L-type breakwater combined with a WEC, which includes an FB of rectangular geometry equipped with an anchored vertical curtain-type wall anchored by piles. Guo et al. (2022) investigated the effects of a porous vertical wall on a submerged, flexible, perforated membrane situated above a varying seabed.

Chen et al. (2020) conducted a numerical investigation into the hydrodynamic efficiency of an FB, which was designed as a vertical pile-restrained WEC. Wang et al. (2022b) conducted a numerical study to investigate breaking wave impact, focusing on wave profile during impact, the pressure exerted by breaking waves, and the interplay between waves and breakwaters with perforations. Cheng et al. (2024) presented a comprehensive approach that combines multiple OWCs with an adaptable FB to harness wave energy. Xu et al. (2022) conducted a review of the latest advancements in wave energy marine buoys, while the aspects of mooring design are discussed by Xu et al. (2019).

Prior research conducted by Mohapatra et al. (2024a) and Islam et al. (2018, 2019) examined wave radiation from a floating rectangular box using an analytical approach in two-dimensional, oblique, and three-dimensional contexts, without incorporating a vertical wall. Conversely, a three-dimensional theoretical model was created to analyze wave interaction with a horizontally floating flexible membrane moored by springs, and this model was compared against experimental test results (Mohapatra et al., 2023). Recently, Mohapatra et al. (2024b) developed a theoretical model of a horizontal floating flexible membrane in a 3D channel, and results are compared with experimental data sets, applications to WEC and breakwater. Amouzadrad et al. (2024) reviewed the hydrodynamics and gap resonance of multi-body floating structures based on analytical and numerical approaches.

Existing theoretical studies lack a comprehensive investigation into the oblique wave interaction between a rectangular heaving buoy WEC and in the presence of a vertical flexible perforated membrane (VFPM) wall.

Hence, Section 2 introduces a mathematical model developed under linearized wave theory and incorporates the VFPM to describe oblique wave radiation from a rectangular box. In Section 3, radiation potentials are derived via Fourier and eigenfunction expansion. These and the diffraction potential enable the calculation of wave excitation force and hydrodynamic coefficients. The mathematical expressions for the heaving buoy's motion and power capture, concerning damping PTO, are also given. In Section 4, the accuracy of the present theoretical result for hydrodynamic coefficients is analysed at various oblique angles, and the results, achieved without incorporating a VFPM wall and a limiting case of vertical rigid perforated wall, are validated by comparison to existing BEM results. In addition, the effects of oblique wave angles and structural design on hydrodynamic coefficients, wave forces, power capture, optimal PTO damping, and transmission coefficients are investigated through numerical results, which are then presented and analysed in detail. Finally, in Section 5, significant concluding remarks and the future direction of the current analysis are discussed.

2 Mathematical formulation

The physical problem is represented by a mathematical model in a 3D Cartesian coordinate system (x, y, z), where the $x - z$ lies in the horizontal plane that lines up with the undisturbed water surface, and vertically downward is considered the positive direction for the y-axis. The new WES consists of a heaving floating box and a VFPM wall is placed after the right end of the floating box at a distance l_1 is connected by the spring moorings with stiffness q. The origin O is considered to be the central point of the rectangular box.

Hence, the distance between the origin O and the vertical membrane is $l + l_1$. The wave radiation arises from the heaving movement of a rectangular box that is floating on a water surface, with a width of $2l$, a draft of d, and extending infinitely in the z-direction. Therefore, the entire fluid domain is categorized into four zones as established by: $x \in (-l, -\infty)$, $x \in (0, h)$, $x \in (-l, l)$, $y \in (d, h)$, $x \in (l, < l + l_1)$, $y \in (0, h)$, and $x \in (l + l_1, \infty), y \in (0, h)$ are referred to as Ω_1, Ω_2, Ω_3, and Ω_4, respectively (as illustrated in Figure 1).

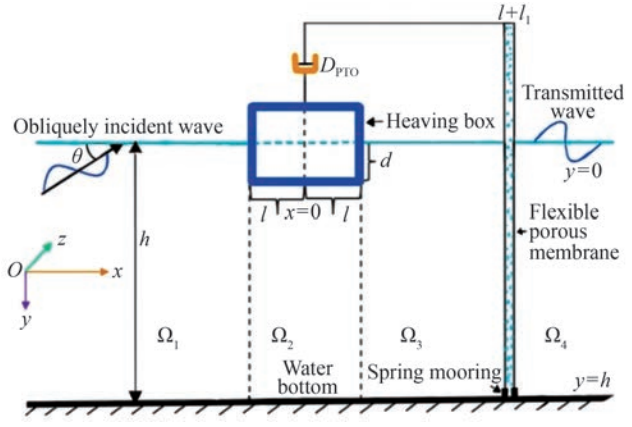

Figure 1 The model of a wave energy extraction system

It is assumed that the water is inviscid and incompressible, with the flow being irrotational and exhibiting simple harmonic motion over time, characterized by an angular frequency ω, as well as in the z-direction.

Therefore, a velocity potential exists $\Phi(x, y, z, t) = \mathrm{Re}\{\phi(x, y, z)\exp(-\mathrm{i}\omega t)\}$, where Re denotes the real part of the complex expression and $\phi(x, y, z)$ denotes the spatial velocity potential. The potential $\phi(x, y, z)$ can be divided into three components: potential attributable to the incoming, the diffracted, and the radiated potentials. These components are indicated by ϕ_I, ϕ_D, ϕ_R respectively. Hence, the global potential ϕ can be written as

$$\phi = \phi_A + \phi_D + \phi_R \tag{1}$$

A progressive wave, characterized by its angular frequency ω, interacts with a rectangular box and it is positioned at an angle θ relative to the x-axis. The spatial velocity potential due to the incident wave resulting from this wave interaction is given by $\phi_A(x, y, z) = \varphi_A(x, y)\mathrm{e}^{\mathrm{i}\gamma z}$, $\gamma = k_0 \sin\theta$, where k_0 represents the z-component of the wavenumber linked with the incident wave. Consequently, the potential of the incident wave for linear waves traveling in the negative x-direction is indicated as

$$\varphi_A = \frac{\mathrm{i}gA}{\omega}\frac{\cosh k_0(h - y)}{\cosh k_0 h}\mathrm{e}^{-\mathrm{i}sx} \tag{2}$$

with g represents the gravitational constant, A (= one half of the wave height = $H/2$ denotes the amplitude of the incoming wave, H denotes the wave height, and for the sake of simplicity in numerical computation, A is assumed to be equal to 1 without any loss of generality, and $s = k_0\cos\theta$ is the x-component of the wave number k_0 related to the incident wave fulfils the dispersion relation as follows.

$$\omega^2 = gk_0 \tanh(k_0 h) \tag{3}$$

Considering that the box's movement is minimal and its oscillations fluctuate sinusoidally in the z-direction, we represent the amplitude of the box's heave motion as I_R. Consequently, the radiated potential, denoted as ϕ_R, is formulated as follows:

$$\phi_R(x, y, z) = -\mathrm{i}\omega I_R \varphi_R(x, y)\mathrm{e}^{\mathrm{i}\gamma z} \tag{4}$$

with φ_R that does not depend on z and associated with the reduced wave equation.

$$\left(\frac{\partial^2}{\partial x^2} + \frac{\partial^2}{\partial y^2} - \gamma^2\right)\varphi_R = 0 \text{ in the fluid domain} \tag{5}$$

The free surface condition can be read as

$$\frac{\partial \varphi_R}{\partial y} + \varepsilon\varphi_R = 0 \text{ on } y = 0 \text{ for } \Omega_1, \Omega_3, \text{ and } \Omega_4 \tag{6}$$

where $\varepsilon = \omega^2/g$.

The conditions at the solid bottom are indicated by

$$\frac{\partial \varphi_R}{\partial y} = 0 \text{ on } y = h \text{ for } \Omega_1, \Omega_2, \Omega_3, \text{ and } \Omega_4 \tag{7a}$$

$$\frac{\partial \varphi_R}{\partial x} = 0 \text{ on } x = l \tag{7b}$$

The boundary condition (BC) resulting from the heaving box is expressed as (see Islam et al., 2019)

$$\frac{\partial \varphi_R}{\partial y} = 1 \text{ on } x \in [-l, l], y = d \tag{8}$$

The term governing the rigid structural boundary is defined by

$$\frac{\partial \varphi_R}{\partial x} = 0, \text{ at } x = \pm l,\ 0 < y < d \tag{9}$$

The linear kinematic and dynamic conditions on the VFPM can be expressed as

$$\frac{\partial \varphi_{R3}}{\partial y} = \frac{\partial \varphi_{R4}}{\partial y} = -\mathrm{i}\omega\xi + \mathrm{i}k_0\sigma\left(\varphi_{R3} - \varphi_{R4}\right) \tag{10a}$$

$$\tau_f\left(\frac{\partial^2}{\partial y^2} + \frac{\partial^2}{\partial z^2}\right)\xi - m_m\frac{\partial^2 \xi}{\partial t^2} = -\left(P_3 - P_4\right) \tag{10b}$$

with $P_j(x, y, z, t) = -\rho g y - \rho\left(\partial\Phi_j/\partial t\right), j = 3, 4$ is the hydrodynamic pressure.

Since the VPFM is tethered to the seafloor via spring moorings, the boundary constraints on the VFPM at $y = 0, h$ are defined by:

$$\tau_f\frac{\mathrm{d}\xi}{\mathrm{d}y} - q\xi = 0, \text{ at } x = l + l_1 \tag{10c}$$

with m_m, τ_f, σ, and ξ refer to the mass density, the membrane tension, the porous-effect parameter, and the membrane displacement of the VFPM, respectively.

It is considered that the far-field condition can take the following form

$$\lim_{x \to \pm\infty}\left(\frac{\partial \varphi_R}{\partial x} \pm \mathrm{i}s\varphi_R\right) = 0 \tag{11}$$

3 Method of solution

Applying the method of variable separation across four distinct zones $\Omega_1, \Omega_2, \Omega_3$, and Ω_4, the radiated potentials φ_R satisfying (5), (6)–(11) are expressed

$$\varphi_{R1} = A_{10}\mathrm{e}^{\mathrm{i}s_0(x+l)}P_0(y) + \sum_{n=1}^{\infty}A_{1n}\mathrm{e}^{\mathrm{i}s_n(x+l)}P_n(y) \tag{12}$$

$$\varphi_{R2} = f(\alpha_0, y) + \sum_{n=0}^{\infty}\left[A_{2n}\mathrm{e}^{-\alpha_n(x+l)} + B_{2n}\mathrm{e}^{\alpha_n(x-l)}\right]Q_n(y) \tag{13}$$

$$\varphi_{R3} = A_{30}\mathrm{e}^{-\mathrm{i}\lambda_0(x-l-l_1)}R_0(y) + \sum_{n=1}^{\infty}A_{3n}\mathrm{e}^{\lambda_n(x-l-l_1)}R_n(y) \tag{14}$$

$$\varphi_{R4} = T_{40}\mathrm{e}^{\mathrm{i}\lambda_0(x-l-l_1)}R_0(y) + \sum_{n=1}^{\infty}T_{4n}\mathrm{e}^{\lambda_n(x-l-l_1)}w_n(y)R_n \tag{15}$$

where $f(\alpha_0, y) = \left\{-\cosh\alpha_0(h-y)\right\}\big/\left\{\alpha_0\sinh\alpha_0(h-d)\right\}$

$$P_0(y) = \frac{\cosh k_0(h-y)}{\cosh k_0 h},\ P_n(y) = \frac{\cos k_n(h-y)}{\cos k_n h} \tag{16}$$

$$Q_n(y) = \cos\beta_n(h-y) \tag{17}$$

$$R_0(y) = \frac{\cosh\mu_0(h-y)}{\cosh\mu_0 h}, \text{ and } R_n(y) = \frac{\cos\mu_n(h-y)}{\cos\mu_n h} \tag{18}$$

with $P_n(y)$'s, $Q_n(y)$'s and $R_n(y)$'s are the eigenfunctions.

The eigenvalues k_0 are defined identically as stated in Equation (3) and $k_n = \mathrm{i}k_n$, s_n, α_n, β_n, and μ_n's that adhere to these dispersion relations include:

$$\omega^2 = -gk_n\tan(k_n h) \tag{19}$$

$$s_n = \begin{cases} k_0\cos\theta & \text{for } n = 0 \\ \sqrt{k_n^2 + \gamma^2} & \text{for } n = 1, 2, \cdots \end{cases} \tag{20}$$

$$\alpha_n = \begin{cases} k_0\sin\theta, & n = 0 \\ \sqrt{\beta_n^2 + \gamma^2}, & n = 1, 2, \cdots \end{cases} \tag{21}$$

$$\beta_n = \frac{n\pi}{(h-d)}, n = 0, 1, 2, \cdots \tag{22}$$

$$\omega^2 = \begin{cases} g\mu_0\tanh(\mu_0 h), & \text{for } n = 0 \\ -g\mu_n\tan(\mu_n h), & \text{for } n = 1, 2, \cdots \end{cases} \tag{23}$$

$$\lambda_n = \begin{cases} \mu_0\cos\theta, & \text{for } n = 0 \\ \sqrt{\mu_n^2 + \gamma^2}, & \text{for } n = 1, 2, \cdots \end{cases} \tag{24}$$

The eigenfunctions $\left(P_n(y)\text{'s}, Q_n(y)\text{'s}, \text{and } R_n(y)\text{'s}\right)$ exhibit orthogonality within their respective intervals (see Mohapatra et al., 2024a).

The continuity of velocity at $x = \pm l$ can be read as

$$\frac{\partial \varphi_{R1}}{\partial x} = \begin{cases} 0, & y \in (0, d) \\ \dfrac{\partial \varphi_{R2}}{\partial x}, & y \in (d, h) \end{cases} \tag{25a}$$

$$\frac{\partial \varphi_{R3}}{\partial x} = \begin{cases} 0, & y \in (0, d) \\ \dfrac{\partial \varphi_{R2}}{\partial x}, & y \in (d, h) \end{cases} \tag{25b}$$

Further, the continuity of pressure at $x = \pm l$ can be read as

$$\varphi_{R1} = \varphi_{R2}, x = l, y \in (d, h) \tag{26a}$$

$$\varphi_{R2} = \varphi_{R3}, x = -l, y \in (d, h) \tag{26b}$$

and by applying the orthogonal relations, a linear system of equations $4(N+1)$ is derived to determine the unknown constants A_{1n}'s, A_{2n}'s, A_{3n}'s and B_{2n}'s.

Proceeding as in Mohapatra et al. (2024a), the system of

linear equations $4(N+1)$ solved by developing MATLAB codes by trimming the infinite series into a finite number of terms N in the expansion as in Equations (12)–(15). Once the unknown coefficients are obtained, then the complete solution will be obtained concerning radiated potentials.

By substituting the velocity potentials φ_{R3} and φ_{R4}, as defined in Equations (17) and (18), into the normal velocity continuity condition on the left-hand side of Equation (13b), we arrive at an equation for the unknown variables for $n = 0, 1, 2, \cdots$ as

$$T_n = A_{3n} \tag{27}$$

3.1 Wave excitation force

Since the floating box is considered infinite in the z-direction and the potential exhibits periodicity in that direction, it is necessary to deal exclusively with the wave-induced forces on a cross-section that is orthogonal to the z-axis. Therefore, the wave forces can be articulated in relation to the incident and radiated potentials as follows:

$$F_e = \mathrm{i}\rho\omega\left[\int_{W_s}\varphi_A(x,y)n\mathrm{d}s - \int_{W_s}\varphi_R(x,y)\frac{\partial\varphi_A}{\partial n}\mathrm{d}s\right] \tag{28}$$

In this context, W_S represents the wetted surface in the xy-plane, while n indicates the inward normal to the floating box within the same plane, defined as $n = n_y$, where n_y signifies the components of the outward-pointing unit normal to the surface of the box.

The dimensionless wave force of heave can be computed by using the following formula.

$$F_v = \frac{|F_e|}{(2\rho g l I_R)} \tag{29}$$

The dimensionless heave added mass (C) and heave damping coefficient (D) are expressed as

$$C = \frac{\mathrm{Re}\left(\rho\int_{-l}^{l}\phi_{R2}\mathrm{d}x\right)}{(2\rho l d)} \tag{30}$$

$$D = \frac{\mathrm{Im}\left(\rho\omega\int_{-l}^{l}\phi_{R2}\mathrm{d}x\right)}{(2\rho\omega l d)} \tag{31}$$

3.2 Power capture and efficiency of the system

The motion of the rectangular box is described by

$$\left[-\omega^2(M+C) - \mathrm{i}\omega(D+D_{\mathrm{PTO}}) + K\right]I_R = F_v \tag{32}$$

with $M = \rho B d$, $K = \rho g B$, and D_{PTO} constitute the buoy mass, hydrostatic spring stiffness, and PTO damping, respectively. Moreover, the symbols C, D, I_R, and F_v have been previously defined.

The calculation of the optimal PTO damping D_{OPTO} for the heaving buoy are presented as (Wang et al., 2022b)

$$D_{\mathrm{OPTO}} = \left[\left\{\frac{K}{\omega} - \omega(M+C)\right\}^2 + D^2\right]^{1/2} \tag{33}$$

The power harnessed by the rectangular buoy is computed as

$$P_{\mathrm{capture}} = 0.5 D_{\mathrm{PTO}}\omega^2\left|I_R^2\right| \tag{34}$$

Conversely, the VFPM's transmission coefficient, K_t, is determined by

$$K_t = \left|\frac{T_0 \mathrm{e}^{\mathrm{i}\lambda_0(l+l_1)}}{\left\{\left(-\mathrm{i}gI_R\right)/\omega\right\}}\right| \tag{35}$$

4 Numerical results and analysis

This section analyses validation of the current solution, several crucial parameters on the hydrodynamic coefficients, the efficiency of capturing power, and the VFPM wall's energy transmission characteristics.

MATLAB R2023b (64-bit, win64) with a desktop PC, equipped with an Intel® Core i7-4790 CPU running at 3.60 GHz, 16 GB of RAM with a frequency of 3 601 MHz, 4 physical cores, and 8 logical processors, and an SSD drive was used to perform the study. The evaluated time for each calculation was between 8 and 10 minutes.

4.1 Convergence analysis and validation

The hydrodynamic coefficients values are accurate to 3-decimal places when N is 30 or greater, as shown in Table 1. Therefore, to ensure numerical accuracy, the calculation of the radiation velocity potential formulas is limited to 30 terms.

Hereafter, all computations are carried out using the current solution and incorporating the water density ρ = 1025 kg/m^3, gravitational constant g = 9.8 m/s, d/h = 0.4, l/h = 0.42, and incident angle $\theta = 30°$ unless otherwise stated.

Figure 2 presents a validation of the current solution for the vertical wave force (F_v) on a heaving box (without a VFPM wall) against BEM results from Zheng et al. (2006), plotted against the non-dimensional wavenumber $k_0 h$. The current results for the vertical force, in the absence of a VFPM wall, demonstrate strong agreement with the BEM data.

Table 1 Convergence study of C and D with $d/h = 0.5$ and $l/h = 0.42$

Oblique angle	N	Added mass (C)	Damping coefficient (D)
$\theta = 30°$	4	0.36539	1.62682
	8	0.37338	1.62637
	12	0.37730	1.62615
	16	0.37804	1.62611
	22	0.37955	1.62602
	26	0.37980	1.62600
	30	0.38025	1.62598
	31	0.38022	1.62598
$\theta = 45°$	4	0.39731	1.98953
	8	0.40528	1.98890
	12	0.40918	1.98860
	16	0.40993	1.98854
	22	0.41143	1.98842
	26	0.41168	1.98840
	30	0.41213	1.98836
	31	0.41210	1.98837
$\theta = 60°$	4	0.49290	2.80515
	8	0.50081	2.80417
	12	0.50468	2.80369
	16	0.50542	2.80360
	22	0.50691	2.80341
	26	0.50716	2.80338
	30	0.50761	2.80333
	31	0.50757	2.80333

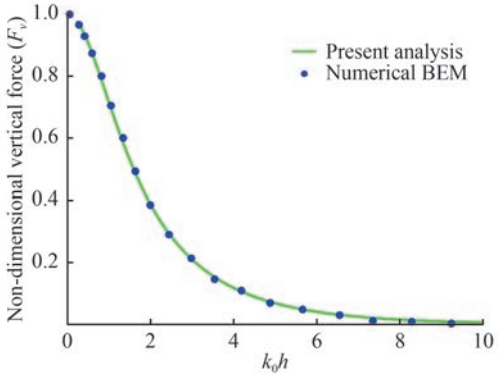

Figure 2 Validation for F_v between the current and that gained via BEM

The non-dimensional added mass A (no VFPM wall) from the current solution is compared to the BEM results of Zheng et al. (2006) in Figure 3, as a function of k_0h. The excellent agreement between the analytical solution and the BEM results validates the present approach, and the solution also captures the trend observed in the BEM data.

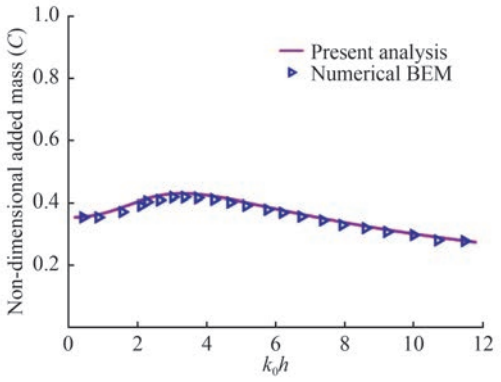

Figure 3 Validation of C between the present and those obtained from a BEM

Figure 4 shows a comparison between the damping coefficient (D) obtained from the current analytical model (without a VFPM wall) and the BEM results of Zheng et al. (2006), plotted against k_0h. The results demonstrate a good agreement in both their trends and numerical values.

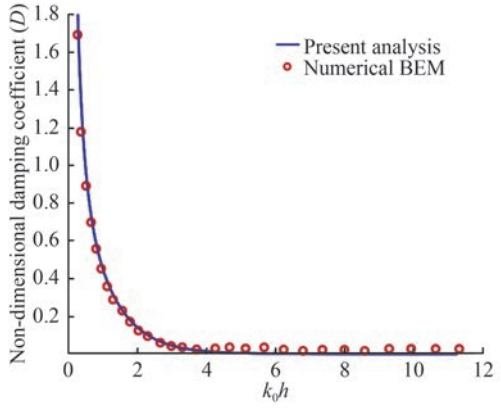

Figure 4 Validation of D between the current results and those obtained from a BEM

In Figure 5, the present solution of the transmission coefficient K_t is validated with a limiting case with incident angle $\theta = 0°$, $l/h = 0$, $d/h = 0$, and a rigid porous wall; existing in the literature (Wang et al., 2022b) versus k_0h. It is observed that they aligned well with their pattern and data points.

4.2 Influence of oblique angle and structural parameters

Figure 6 presents the influence of obliquely incident angle θ on the F_v against k_0h. It has been noted that as the values of θ increase, the vertical wave force diminishes. This suggests that the angle of the incoming wave aligns parallel to the floating box, resulting in a diminished effect.

Figure 7 simulates the impact of d/h on the dimensionless vertical wave force (F_v) for $l/h = 0.18$ and oblique angle $\theta = 30°$ against k_0h. It can be seen that the values of F_v

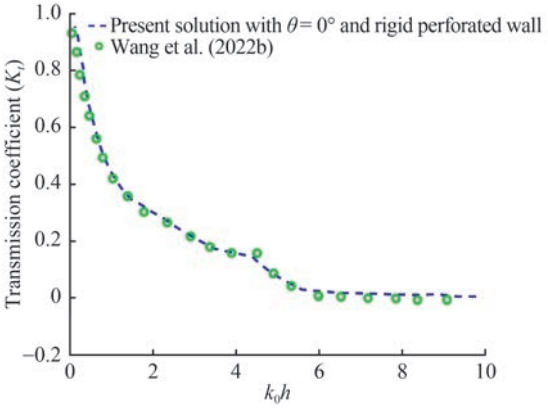

Figure 5 Comparison of K_t between the present and a limiting case; rigid perforated wall

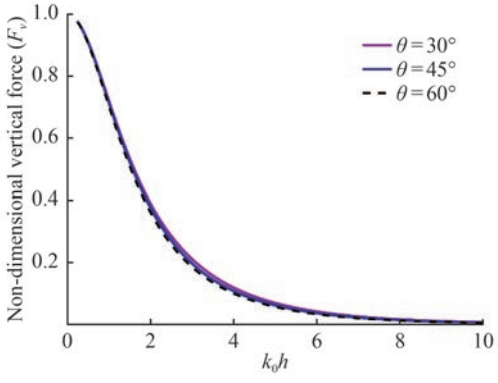

Figure 6 Influence of θ on the F_v versus k_0h

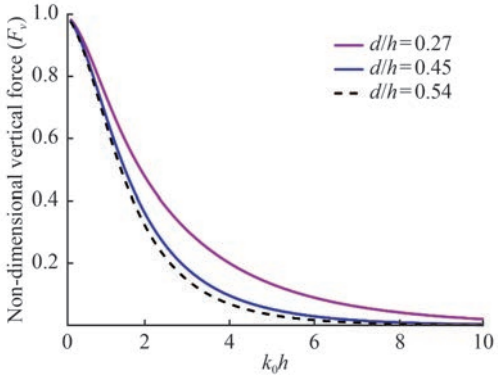

Figure 7 Effect of d/h on the F_v versus k_0h

increase with a decrease in d/h. The reason is that the deeper drafts create greater horizontal loads on the floating box while resulting in smaller vertical loads.

Figure 8 demonstrates the influences of l/h on the F_v for d/h = 0.4 and θ = 30° against k_0h. It has been noted that the vertical wave forces rise as the width of the box increases. Figure 9 demonstrates the impact of θ on the A for d/h = 0.4 and h/l = 6 against k_0h. The added mass rises with θ at lower wavenumbers, k_0h but this trend reverses at larger wavenumbers.

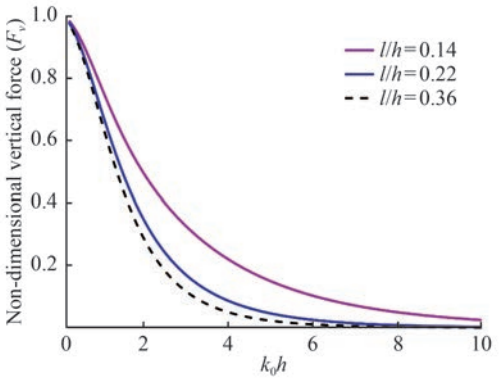

Figure 8 Influence of l/h on the F_v versus k_0h

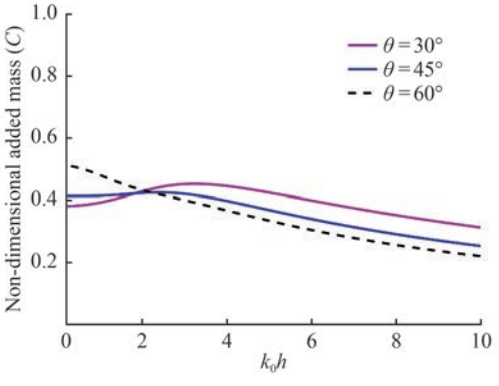

Figure 9 Effect of θ on the added mass versus wavenumber

In Figure 10, the effects of non-dimensional draft d/h on the non-dimensional added mass of the heave, with l/h = 0.18 and oblique angle. versus k_0h are plotted. It is observed that the added mass of heave decreases with an increase in non-dimensional draft d/h, which is due to the fact that higher in the draft yields larger in the mass of the structure, thus, the heave structure resonates less in heave motions.

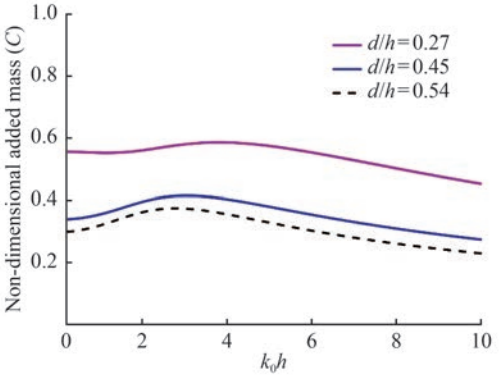

Figure 10 Influence of d on C vs. the wavenumber

Figure 11 gives the impact of non-dimensional width l/h on the C, with d/h = 0.18 and oblique angle θ = 30° versus k_0h are plotted. The added mass of heave is observed to decrease as the values of l/h increases for $k_0h \geqslant 5$. However, this pattern does not consistently hold for smaller values k_0h.

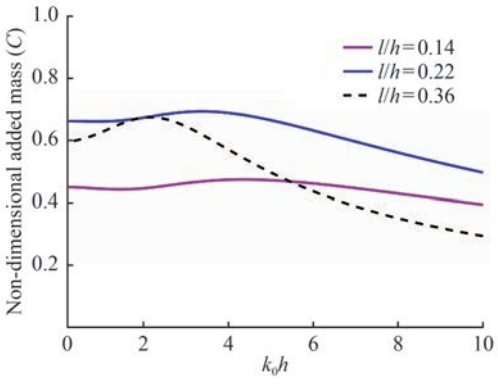

Figure 11 Influence of l/h on the added mass against the wavenumber

Figure 12 reveals observations similar to those in Figure 6. Nevertheless, at larger k_0h, the damping coefficients (D) exhibit negligible variation across various oblique angles, effectively approaching zero. Figure 13 illustrates the relationship between the non-dimensional draft d/h and the D, plotted against k_0h for l/h = 0.18. The plots show that as the structural draft increases, the heave damping coefficients diminish.

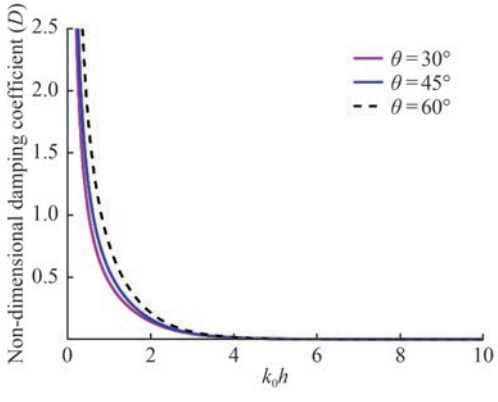

Figure 12 Influence of θ on the damping coefficient D versus k_0h

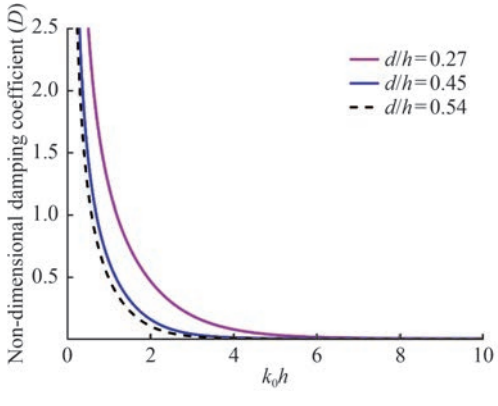

Figure 13 Effect of d/l on D versus k_0h

In Figure 14, the damping coefficients of heave become lower for longer structures. This occurs because, as the structural length increases while the draft and width remain constant, the mass of the structure also rises, resulting in reduced damping.

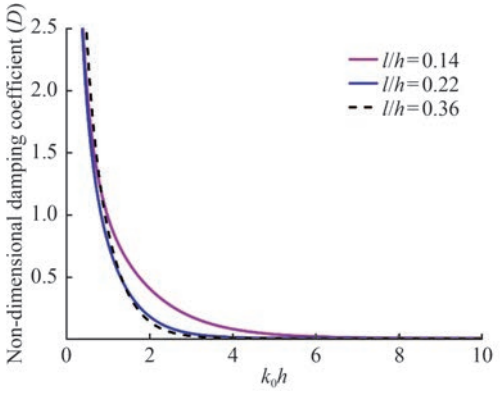

Figure 14 Effect of l/h on D versus wavenumber

4.3 Impact of oblique angle and structure parameters on the Pcapture and PTO damping

Figure 15 illustrates the relationship between oblique wave angle and the P_{capture} as a function of k_0h with d/h = 0.4 and l/h = 0.18. The plots show that as θ increases, the WEC captures more power at lower k_0h. However, this fashion reverses at higher k_0h.

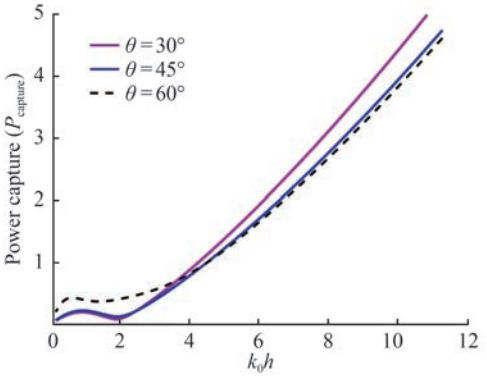

Figure 15 Influence of oblique angle θ on the power capture

Also, in Figure 15, wave-capturing power is more significant in shallower water compared to deeper water. This recommends that such a wave energy system could be particularly effective in coastal regions for energy extraction.

Figures 16–17, the influence of the nondimensional draft and the width of the box on the P_{capture} for oblique wave angle θ = 30° versus k_0h are plotted. In both cases, it was seen that the power captured by the WEC becomes greater for the higher draft and wider structure as the wavenumber increases. However, this effect seems to be negligible for smaller wavenumber. This suggests that this type of wave energy system may be more effective for extracting wave energy in coastal areas.

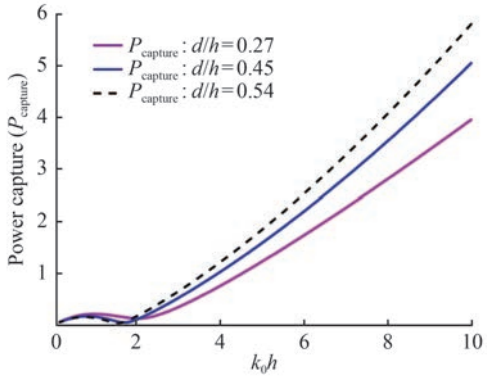

Figure 16 Effect of d/h on the power capture with l/h = 0.18 and θ = 30°

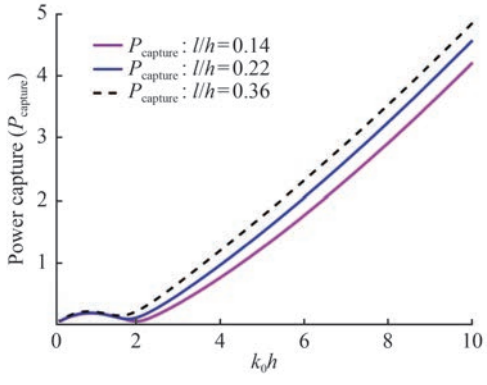

Figure 17 Effect of l/h on the power capture with d/h=0.4 and θ = 30°

The effect of θ on the optimal PTO damping coefficient versus k_0h is shown in Figure 18. The results indicate that higher θ lead to increased optimal damping. Nevertheless, at higher k_0h, this increase diminishes slightly, exhibiting a minor reversal. In Figures 19–20, the impact of structural parameters (draft and width) on the optimal PTO damping with d/h = 0.4 and θ = 30° versus k_0h are illustrated. The observations resemble those shown in Figure 16 and Figure 17.

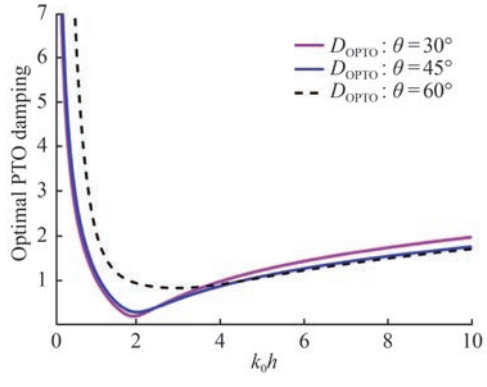

Figure 18 Impact of θ on the optimal PTO damping

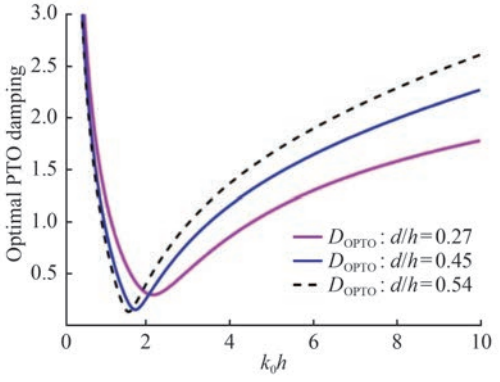

Figure 19 Effect of d/h on the optimal PTO damping for θ = 30°

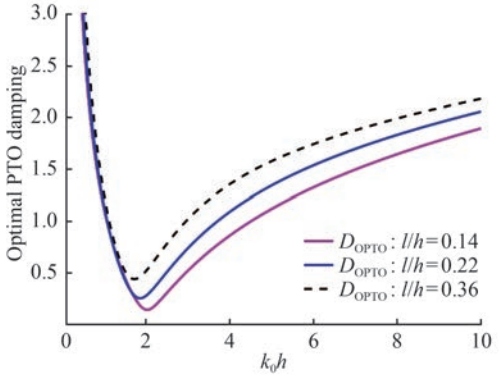

Figure 20 Effect of l/h on the optimal PTO damping versus k_0h

4.4 Effect of oblique angle and design parameters on transmission coefficients

Figures 21–23 present the impact of various oblique angles, non-dimensional structural draft, and width on the transmission coefficients K_t versus k_0h. It is seen that as the incidence angle, draft, and width of the structure increase the transmission coefficient becomes lower. Further, with larger values of wavenumber, the impact of angle and structural parameters on the K_t is minimal.

In Figure 24, the impact of porous-effect parameter on the

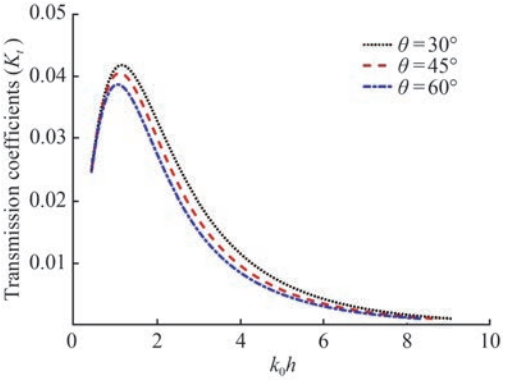

Figure 21 Influence of θ on the transmission coefficients

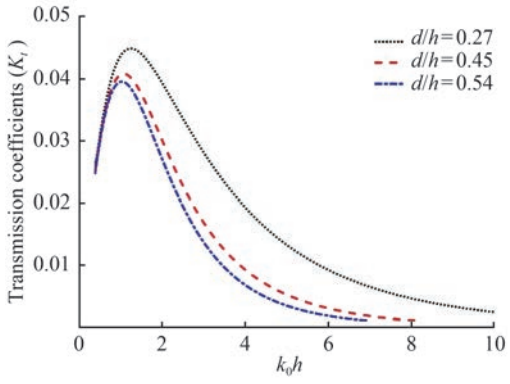

Figure 22 Impact of the structural draft on K_t vs. k_0h

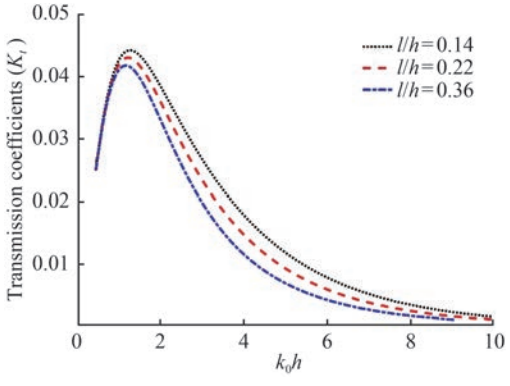

Figure 23 Impact of structural width on the K_t

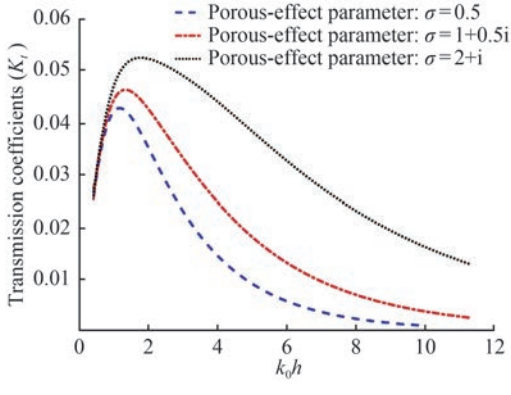

Figure 24 Influence of porous-effect parameter σ on the K_t

K_t is analyzed. Three values are used for the porous effect parameter σ. The second and third of these values included coefficients for both inertial and frictional resistance. It is found that as the values of σ rises the K_t becomes higher. Also, it can be observed that the when both exist (inertial and frictional resistance) in the porous effect parameter that gives a greater performance in wave transmission than that the case of only inertial force exist.

5 Conclusions

This study introduces a mathematical model that illustrates a WES comprised of a floating rectangular heaving box and a moored, VFPM wall subjected to oblique waves. The eigenfunction expansion method and the orthogonal condition are used to derive the analytical expressions of the radiated potentials in each region. The hydrodynamic coefficients, the motion equation, and the power capture formulas related to the damping PTO are provided. The accuracy of the analytical results for the hydrodynamic coefficients on different oblique angles is demonstrated and the efficiency of the power capture on the influence of oblique wave angles is examined. The analysis leads to the following key conclusions:

1) The paper offers a novel contribution through the integration of a moored VFPM wall with a floating rectangular heaving box, specifically addressing the scenario of oblique wave conditions and analysing the impact of these waves on hydrodynamic coefficients and wave power. In addition, the current results concerning hydrodynamic coefficients and wave quantity were consistent with prior findings.

2) It has been found that as the oblique angle increases, both the vertical wave force added mass and the damping coefficient decrease. The power harnessed by the rectangular buoy is substantial in coastal areas; however, as the incidence angle increases, the ideal PTO damping rises for smaller values of k_0h.

3) Regarding the transmission coefficients, it is found that the oblique angle and structural parameters play a vital role in the transmission of waves below the rectangular buoy.

4) This analysis could aid in understanding the hydrodynamic performance of WEC concerning their PTO systems. This formulation and analysis could contribute to developing an integrated WES, featuring a combination of an array of heaving buoys and a moored flexible perforated membrane wall under current load.

Funding Open access funding provided by FCT|FCCN (b-on).

Acknowledgement This work contributes to the Strategic Research Plan of the Centre for Marine Technology and Ocean Engineering (CENTEC), which is financed by the Portuguese Foundation for Science and Technology (Fundação para a Ciência e Tecnologia-FCT) under contract UIDB/UIDP/00134/2020.

Competing interest C. Guedes Soares is one of Editors for the Journal of Marine Science and Application and was not involved in the editorial review, or the decision to publish this article. Sarat Chandra Mohapatra is an editorial board member for the Journal of Marine Science and Application and were not involved in the editorial review, or the decision to publish this article. All authors declare that there are no other competing interests.

References

Amouzadrad P, Mohapatra SC, Guedes Soares C (2024) Review of recent developments on the hydroelastic response and gap resonance of multi-body floating structures. Ocean Engineering 313: 119398. https://doi.org/10.1016/j.oceaneng.2024.119398

Bhattacharjee J, Guedes Soares C (2011) Oblique wave interaction with a floating structure near a wall with stepped bottom. Ocean Engineering 38: 1528-1544. https://doi.org/10.1016/j.oceaneng.2011.07.011

Chen Q, Zang J, Birchall, Ning DZ, Zhao XL, Gao JL (2020) On the hydrodynamic performance of a vertical pile-restrained WEC-type floating breakwater. Renewable Energy 146: 414-425. https://doi.org/10.1016/j.renene.2019.06.149

Cheng Y, Du W, Dai S, Yuan Z, Incecik A (2024) Wave energy conversion by an array of oscillating water columns deployed along a long-flexible floating breakwater. Renewable and Sustainable Energy Reviews 192: 114206. https://doi.org/10.1016/j.rser.2023.114206

Elchahal G, Younes R, Lafon P (2008) The effects of reflection coefficient of the harbour sidewall on the performance of floating breakwaters. Ocean Engineering 35: 1102-1112. https://doi.org/10.1016/j.oceaneng.2008.04.015

Guo YC, Mohapatra SC, Guedes Soares C (2022) Submerged breakwater of a flexible porous membrane with a vertical flexible porous wall over variable bottom topography. Ocean Engineering 243: 109989. https://doi.org/10.1016/j.oceaneng.2021.109989

Hallak TS, Guedes Soares C (2025) Overview of the recent developments in hybrid floating wind-wave platforms. Journal of Marine Science and Application 24: 98-119. https://doi.org/10.1007/s11804-024-00544-w

Han X, Dong S (2021) Experimental study of wave force on breakwater head under oblique waves. Proceedings of Institution of Mechanical Engineers Part M: Journal of Engineering for the Maritime Environment 236(3): 553-568. https://doi.org/10.1177/14750902221094978

Hsu HH, Wu YC (1997) The hydrodynamic coefficients for an oscillating rectangular structure on a free surface with sidewall. Ocean Engineering 24(2): 177-199. https://doi.org/10.1016/0029-8018(96)00009-1

Islam H, Mohapatra SC, Gadelho J, Guedes Soares C (2019) OpenFOAM analysis of the wave radiation by a box-type floating structure. Ocean Engineering 193: 106532. https://doi.org/10.1016/j.oceaneng.2019.106532

Islam H, Mohapatra SC, Guedes Soares C (2018) Comparison of CFD, experimental and analytical simulations of a heaving box-type floating structure. In: Progress in Maritime Technology and Engineering, Guedes Soares C, Santos TA (Eds.), Taylor & Francis Group, London, 633-639

Ji Q, Xu C, Jiao C (2021) Numerical investigation on the hydrodynamic performance of a vertical pile-restrained reversed L-type floating breakwater integrated with WEC. Ocean Engineering 238: 109635. https://doi.org/10.1016/j.oceaneng.2021.109635

Mohapatra SC, Bispo IB, Guo YC, Guedes Soares C (2024a) Analysis of wave-induced forces on a floating rectangular box with analytical and numerical approaches. Journal of Marine Science and Application 23(1): 113-126. https://doi.org/10.1007/s11804-024-00385-7

Mohapatra SC, Guedes Soares C, Belibassakis K (2024b) Current loads on a horizontal flexible membrane in a 3D channel. Journal of Marine Science and Engineering 12(9): 1583. https://doi.org/10.3390/jmse12091583

Mohapatra SC, Guo YC, Guedes Soares C (2023) Analytical and experimental study on wave interaction with a horizontal floating flexible membrane supporting by linear springs. In: Trends in Renewable Energies Offshore, Guedes Soares, C. (Ed.), Taylor and Francis, London, 257-266

Mustapa MA, Yaakob OB, Ahmed YM, Rheem C, Koh KK, Adnan FA (2017) Wave energy device and breakwater integration: A review. Renewable and Sustainable Energy Reviews 77: 43-58. https://doi.org/10.1016/j.rser.2017.03.110

Ning DZ, Zhao XL, Zhao M, Hann M, Kang HG (2017) Analytical investigation of hydrodynamic performance of a dual pontoon WEC-type breakwater. Applied Ocean Research 65: 102-111. https://doi.org/10.1016/j.apor.2017.03.012

Rezanejad K, Guedes Soares C (2018) Enhancing the primary efficiency of an oscillating water column wave energy converter based on a dual-mass system analogy. Renewable Energy 123: 730-747. https://doi.org/10.1016/j.renene.2018.02.084

Rezanejad K, Guedes Soares C (2021) Hydrodynamic investigation of a novel concept of Oscillating Water Column type wave energy converter device. Journal of Offshore Mechanics and Arctic Engineering 143: 042003. https://doi.org/10.1115/1.4050268

Schay J, Bhattacharjee J, Guedes Soares C (2013) Numerical modelling of a heaving point absorber in front of a vertical wall. 32nd International Conference on Ocean, Offshore and Arctic Engineering (OMAE 2013), Nantes, OMAE2013-11491. https://doi.org/10.1115/OMAE2013-11491

Shen YM, Zheng YH, You YG (2005) On the radiation and diffraction of linear water waves by a rectangular structure over a sill. Part I. Infinite domain of finite water depth. Ocean Engineering 32: 1073-1097. https://doi.org/10.1016/j.oceaneng.2004.07.011

Vicinanza D, Lauro E, Contestabile P, Gisonni C, Lara JL, Losada IJ (2019) Review of innovative harbor breakwaters for wave-energy conversion. Journal of Waterway, Port, Coastal, and Ocean Engineering 145(4): 03119001. https://doi.org/10.1061/(ASCE)WW.1943-5460.0000519

Wang D, Dong S, Fang K (2022a) Breaking wave impact on perforated caisson breakwaters: A numerical investigation. Ocean Engineering 249: 110919. https://doi.org/10.1016/j.oceaneng.2022.110919

Wang Y, Dong S (2021) Theoretical investigation on integrating a torus oscillating body with a concentric perforated cylindrical system. Ocean Engineering 242: 110122. https://doi.org/10.1016/j.oceaneng.2021.110122

Wang Y, Dong S (2023) Theoretical investigation on integrating a heaving WEC in the semicircle opening of a vertical breakwater. Journal of Fluids and Structures 120: 103911. https://doi.org/10.1016/j.jfluidstructs.2023.103911

Wang Y, Wang D, Dong S (2022b) A theoretical model for an integrated wave energy extraction system consisting of a heaving buoy and a perforated wall. Renewable Energy 189: 1086-1101. https://doi.org/10.1016/j.renene.2022.03.052

Xu R, Wang H, Xi Z, Wang W, Xu M (2022) Recent progress on wave energy marine buoys. Journal of Marine Science and Engineering 10(5): 566. https://doi.org/10.3390/jmse10050566

Xu S, Wang S, Guedes Soares C (2019) Review of mooring design for floating wave energy converters. Renewable and Sustainable Energy Reviews 111: 595-621. https://doi.org/10.1016/j.rser.2019.05.027

Zhang H, Zhou B, Vogel C, Willden R, Zang J, Geng J (2020) Hydrodynamic performance of a dual-floater hybrid system combining a floating breakwater and an oscillating-buoy type wave energy converter. Applied Energy 259: 114212. https://doi.org/10.1016/j.apenergy.2019.114212

Zhao XL, Ning DZ, Zou QP, Qiao D, Cai SQ (2019) Hybrid floating breakwater WEC system: a review. Ocean Engineering 186: 106126. https://doi.org/10.1016/j.oceaneng.2019.106126

Zheng YH, Shen YM, You YG, Wu BJ, Jie DS (2006) Wave radiation by a floating rectangular structure in oblique seas. Ocean Engineering 33: 59-81. https://doi.org/10.1016/j.oceaneng.2005.04.005